World Electric Vehicle Journal

MDPI

Article

Dynamic Programming of Electric Vehicle Reservation Charging and Battery Preheating Strategies Considering Time-of-Use Electricity Price

Bo Zhu *, Chengwu Bao, Mingyao Yao * and Zhengchun Qi

School of Automobile and Transportation Engineering, Hefei University of Technology, Hefei 230009, China
* Correspondence: zhubo@hfut.edu.cn (B.Z.); yaomingyao@126.com (M.Y.)

Abstract: Electric vehicles can effectively make use of the time-of-use electricity price to reduce the charging cost. Additionally, using grid power to preheat the battery before departure is particularly important for improving the vehicle mileage and reducing the use cost. In this paper, a dynamic programming algorithm is used to optimize the battery AC (Alternating Current) charging–preheating strategy to minimize the total cost of battery charging and preheating, with the charging current and battery preheating power consumption as the control variables. The cost difference between the optimized control strategy and the conventional preheating strategy was analyzed under different ambient temperatures (−20~0 °C) and different target travel times (7:00~12:00). The simulation results show that the optimized control strategy makes the state of charge (*SOC*) and temperature of the battery reach the set value at the user's target departure time, and the total cost of the grid is the lowest. Compared with the conventional preheating strategy, the optimized control strategy can utilize the power grid energy in the valley price area and reduce the opening time of the positive temperature coefficient (PTC) heater in the flat and the peak price zones. Furthermore, the cost utilization rate can reach 18.41~73.96%, and the cost-saving effect is significant.

Keywords: electric vehicles; battery preheating; reservation charging; dynamic programming; time-of-use electricity price

Citation: Zhu, B.; Bao, C.; Yao, M.; Qi, Z. Dynamic Programming of Electric Vehicle Reservation Charging and Battery Preheating Strategies Considering Time-of-Use Electricity Price. *World Electr. Veh. J.* **2024**, *15*, 90. https://doi.org/10.3390/wevj15030090

Academic Editor: Joeri Van Mierlo

Received: 9 January 2024
Revised: 23 February 2024
Accepted: 27 February 2024
Published: 1 March 2024

1. Introduction

In order to solve the energy crisis and environmental pollution problems, electric vehicles are regarded as a viable alternative to traditional fuel vehicles due to their advantages of energy saving and environmental protection [1,2]. After more than a decade of development, the new energy vehicle industry has achieved large-scale industrialization, and will enter a rapid growth stage. Lithium batteries are widely used in pure electric vehicles due to their advantages of high energy density, low self-discharge rate, energy saving, and environmental protection [3,4]. However, low temperatures still have a significant impact on the performance of electric vehicles. For example, lithium batteries have deteriorated charge–discharge performance, capacity loss, and accelerated life decline in low-temperature environments, which seriously affects the driving range under low-temperature conditions [5]. For example, the actual capacity of a Li-$FePO_4$ battery under −20 °C is only 70% of the same charging condition at 25 °C. Even for a Li-MnO_2 battery with better low-temperature performance, the charging capacity at −20 °C is only about 80% of that at normal temperature. The low temperature reduces the effective power consumption of lithium batteries, which limits the application of electric vehicles in cold northern regions. Therefore, it is essential to heat lithium-ion batteries to ensure they operate within the appropriate temperature range, which can improve their overall performance in low-temperature conditions.

At present, the heating methods of lithium batteries are mainly divided into two categories: internal heating and external heating [6]. Internal heating can be divided into DC (Direct Current) heating, AC (Alternating Current) heating, pulse heating, and other methods [7]. Ruan et al. [8] used a multi-objective genetic algorithm to optimize the DC heating strategy for the two conflicting objectives of battery preheating time and capacity loss. The results show that the battery is rapidly heated from −30 °C to 2.1 °C in 103 s, and the capacity loss of the battery is only 1.4% after 500 reheating cycles, which proves that the method can effectively reduce the capacity loss of the battery. Zhu et al. [9] studied the effects of AC frequency, amplitude, and voltage limits on battery life. The experimental results show that the cell embedded in the thermocouple has good temperature uniformity both inside and on the surface of the lithium battery during the AC heating process. Additionally, under the normal voltage protection limit, even in the low-frequency range (0.5 Hz), the AC heating method will not aggravate the degradation of the battery. Wu et al. [10] proposed an optimization strategy for battery pulse heating to reduce battery capacity decay. The results show that the optimized strategy can heat the lithium battery from −20 °C to 5 °C in 308 s, and the capacity loss is only 0.035% after 30 heating cycles. However, internal heating presents several challenges, including complicated manufacturing of heating equipment, significant battery life decline, and difficulty in ensuring temperature uniformity of large battery packs [11]. External heating methods mainly include air heating [12,13], liquid heating [14], and phase change material heating [15,16]. Luo et al. [17] proposed a preheating scheme combining a supercapacitor and a phase change energy storage system. By adjusting the supercapacitor, the preheating rate of the battery system can reach 69.5 °C/min, and the temperature difference of the battery pack can be controlled within 5 °C. This method can effectively improve the low-temperature response of the energy storage system. Liu et al. [18] developed an optimization model for a battery pack charging strategy based on a liquid thermal management system. By introducing a preheating phase before charging, the charging time was reduced by 16%, and the energy consumption of the heater was decreased by 15%. Liquid heating is widely used in the thermal management circuits of pure electric vehicles due to its advantages of high thermal conductivity, safety and reliability, and easier switching between different thermal management circuits.

Despite the above progress, the battery preheating strategy can be further improved considering the travel needs of users. For example, in the scenario in which the user finishes work one afternoon and travels the next morning, developing a preheating strategy according to the user's travel time is worth considering. Unlike previous studies, considering the time to preheat the battery in this scenario is not very important because there is enough time at night. Due to the high quality of battery packs for pure electric vehicles, battery heating consumes relatively high energy. Utilizing the battery's electrical energy to heat itself is a common method. However, this method will shorten the low-temperature driving range of electric vehicles. In order to save battery energy consumption and improve vehicle driving range, some scholars proposed the use of charging piles to provide energy for battery preheating. Antoun et al. [19] simulated the impact of large-scale electric vehicle preheating on a residential distribution network in a scenario where users use charging piles to precondition cars before traveling. Sørensen et al. [20] considered the use of power grid energy to preheat the cabin and established a multiple linear regression model to study the relationship between various variables and the use of preheating energy. Using a charging pile to preheat the battery can effectively improve the low-temperature charging and discharging performance of the battery, enhance the electric vehicle range, and save the waiting time required to warm up the vehicle, effectively improving the driving experience.

In daily life, the electricity price of the grid fluctuates over time. According to the principle of the lowest electricity cost, the strategy of preheating the battery pack by the charging pile can be adjusted according to the time-of-use (TOU) electricity price. However,

at present, the TOU electricity price is mainly applied to optimizing pure EV charging loads and guiding users' charging and discharging behaviors [21–23]. OuYang et al. [24] proposed a multi-objective optimization charging strategy covering user travel demand, charging cost, energy loss, and other aspects using the time-of-use electricity price. Simulation results show that this strategy not only fully meets the charging needs but also significantly reduces the charging cost and energy loss. However, it only considers the effect of the time-of-use electricity price on the charging cost but does not involve the cost effect of preheating batteries.

To remedy the above defections, this research focuses on how to use the TOU to develop a battery preheating strategy to minimize the cost of electricity. At the same time, in order to make full use of the waste heat generated by the internal resistance of the battery during the charging process, the amplitude of the slow charging current is also optimized based on the TOU price. The rest of this paper is organized as follows. In Section 2, this paper presents a battery thermal management simulation model and a charging model utilizing experimental data from a real pure electric vehicle. In Section 3, the charging and battery preheating strategies under different ambient temperatures and different target departure times are optimized using a dynamic programming algorithm. In Section 4, the feasibility and superiority of the proposed method, in terms of reducing the cost of battery preheating and the target travel time, is verified by comparison with the conventional preheating strategy. Finally, Section 5 concludes this article.

2. Thermal Management System Modeling

2.1. Integrated Thermal Management System Scheme

The integrated thermal management system is shown in Figure 1, and includes three main thermal management system cycles: motor thermal cycle, battery thermal cycle, and cabin heating cycle. The motor thermal cycle includes a motor, MCU, and a pump. By controlling the three-way valve 1, the switching of the internal and external cycles is achieved. For example, the motor coolant flows through the AB port of the three-way valve 1, which can achieve an internal cycle and quickly raise the coolant temperature; the motor coolant flows through the AC port of the three-way valve 1, achieving an external cycle, which can fully utilize the radiator to cool the motor or battery. The battery thermal cycle includes a water–water heat exchanger and a pump, where the heat exchanger is the node between the battery cycle and the cabin heating cycle, using the positive temperature coefficient (PTC) heater to heat the battery. By controlling three-way valve 2, the battery coolant flows from A to C, and the heat exchanger can be used to exchange heat with the PTC heater. The battery coolant flows through the AB port of the three-way valve 2, thereby stopping the battery cycle heating. As this paper mainly focuses on the heating function of batteries, the air conditioning refrigeration circuit is not included in this structure. The cabin heating cycle includes a pump, PTC heater, heater core, and blower. The PTC heater is used to provide heat to the cabin through the heating core. In addition, when the four-way valves AB and CD are connected, the motor thermal cycle and the battery thermal cycle are independent of each other. When the four-way valve AD and BC are connected, the motor thermal cycle and battery thermal cycle are connected in series, which can use the heat from the motor to heat the battery or use the radiator to cool the battery. According to the heating/cooling requirements of the motor, battery, and cabin, the integrated thermal management system scheme has ten operating modes, as shown in Table 1. In addition, the operating state of the main components for each operating mode is shown in Table 2.

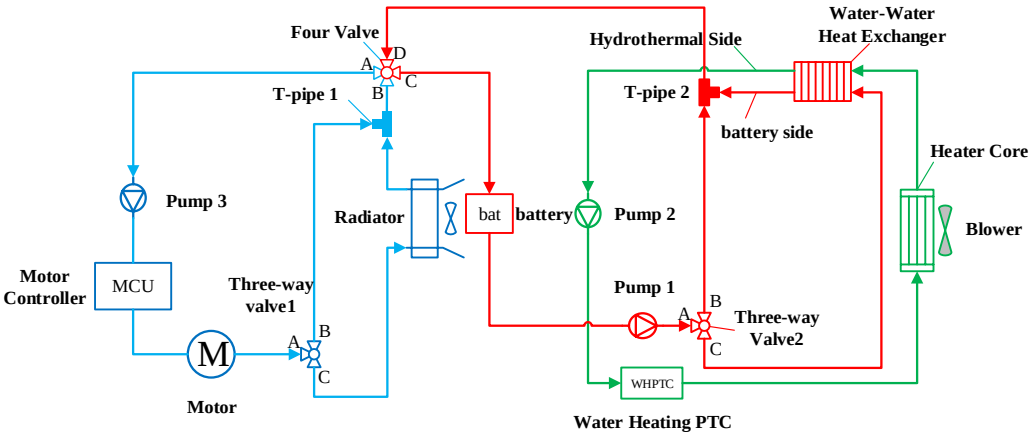

Figure 1. Integrated thermal management system scheme [25].

Table 1. Operating modes of the integrated thermal management system.

Mode	Battery	Motor	Cabin
1	PTC heating	Heat storage	Heating
2	PTC heating	Heat storage	Non-heating
3	Temperature maintenance mode	Cooling	Heating
4	Temperature maintenance mode	Cooling	Heating
5	Temperature maintenance mode	Heat storage	Heating
6	Temperature maintenance mode	Heat storage	Heating
7	PTC heating + waste heat recovery	Waste heat recovery	Heating
8	PTC heating + waste heat recovery	Waste heat recovery	Non-heating
9	Cooling	Cooling	Heating
10	Cooling	Cooling	Non-heating

Table 2. Operating state of main components for each operating mode.

Mode	Pump 1	Pump 2	Pump 3	Three-Way Valve 1	Three-Way Valve 2	Four-Way Valve	Blower
1	1	1	1	AB	AC	AB, CD	1
2	1	1	1	AB	AC	AB, CD	0
3	1	1	1	AC	AB	AB, CD	1
4	1	0	1	AC	AB	AB, CD	0
5	1	1	1	AB	AB	AB, CD	1
6	1	0	1	AB	AB	AB, CD	0
7	1	1	1	AB	AC	AD, BC	1
8	1	1	1	AB	AC	AD, BC	0
9	1	1	1	AC	AB	AD, BC	1
10	1	1	1	AC	AB	AD, BC	0

1 represents "ON" and 0 represents "OFF".

2.2. Battery Model

Compared with the battery first-order RC and electrochemical models, the Rint model requires fewer parameters and is faster to compute [26,27]. As shown in Figure 2, to simplify the model, the battery Rint model is considered in this paper (see Table 3 for the main parameters). The battery pack is assumed to be a mass block with uniform temperature and consists only of an open-circuit voltage source and internal resistance. Therefore, the battery terminal voltage during charging is calculated as:

$$U_T = U_{ocv} + I_{bat} \cdot R_{bat} \quad (1)$$

where U_T is the battery pack terminal voltage, U_{ocv} is the battery pack open circuit voltage, I_{bat} is the battery pack charging current (battery charging current is positive), and R_{bat} is the battery pack charging internal resistance.

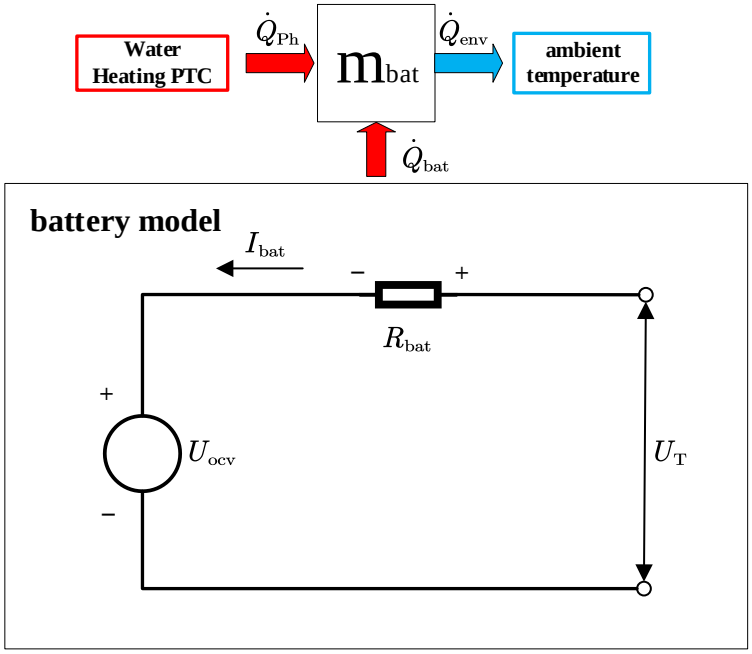

Figure 2. Schematic diagram of the battery model.

Table 3. Main parameters of battery pack.

Parameters	Value	Unit
Total mass	240	kg
Specific heat capacity	1140	j/(kg·k)
Capacity	163	A·h
Heat exchange area	0.7474	m^2
Heat transfer coefficient	10	$W/(m^2 \cdot K)$
Cumulative heating efficiency	0.9	—
Series-parallel connection	96S1P	—

Li-ion batteries' internal resistance and open-circuit voltage are nonlinear functions of temperature and *SOC*, and the temperature and *SOC* of the battery are correlated with battery charging–preheating costs. Therefore, modeling of battery heat production and charging is required. The thermodynamic processes of the battery pack in the low-temperature charging–preheating scenario mainly include:

- Heat production by the internal resistance of the battery;
- Effective heating by the PTC heater;
- Heat transfer between the battery pack and the environment.

The effective heat transferred to the battery can be divided into two parts: one part is used for heating the battery mass block, and the other is dissipated into the environment. Thus, the battery heat balance equation is as follows:

$$\dot{Q}_{bat} + \dot{Q}_{Ph} - \dot{Q}_{env} = c \cdot m \cdot \dot{T}_{bat} \quad (2)$$

where $\dot{Q}_{bat}$ is the heat-generating power of the battery pack, $\dot{Q}_{Ph}$ is the effective power of the PTC heater, $\dot{Q}_{env}$ is the heat exchange power between the battery pack and the environment, c is the specific heat capacity of the battery pack, m is the total mass of the battery pack, and $\dot{T}_{bat}$ is the average temperature of the battery pack.

Taking into account $\dot{Q}_{\mathrm{bat}} = {I_{\mathrm{bat}}}^2 \cdot R_{\mathrm{bat}}$, $\dot{Q}_{\mathrm{Ph}} = P_{\mathrm{h}} \cdot \eta_{\mathrm{ptc}}$, and $\dot{Q}_{\mathrm{env}} = \mathrm{h} \cdot \mathrm{A} \cdot (T_{\mathrm{bat}} - \mathrm{T_{env}})$, the specific expression for Equation (2) is as follows:

$$ {I_{\mathrm{bat}}}^2 \cdot R_{\mathrm{bat}} + P_{\mathrm{h}} \cdot \eta_{\mathrm{ptc}} - \mathrm{h} \cdot \mathrm{A} \cdot (T_{\mathrm{bat}} - \mathrm{T_{env}}) = \mathrm{c} \cdot \mathrm{m} \cdot \dot{T}_{bat} \tag{3} $$

where P_{h} is the electric power of the PTC heater, η_{ptc} is the cumulative heating efficiency of the PTC heater and the water–water heat exchanger, h is the heat transfer coefficient of the battery pack, A is the heat exchange area of the battery pack, and $\mathrm{T_{env}}$ is the ambient temperature.

The *SOC* of the battery during the charging process is related to the charging current, and its expression is as follows:

$$ \dot{SOC} = \frac{I_{\mathrm{bat}}}{Q_{\mathrm{bat}} \cdot 3600} \tag{4} $$

where Q_{bat} is the battery pack capacity.

3. Battery AC Charge–Preheat Strategy

3.1. Optimal Control Modeling

The main objective of this paper is to reasonably utilize grid energy from charging stations to charge and preheat pure electric vehicle batteries. The aim is to guarantee that the batteries attain the desired state of charge and the temperature for the user's target departure time while minimizing the overall energy consumption cost from the grid. The working conditions of the time-of-use electricity price are fixed, and mainly include valley, flat, and peak price zones, as shown in Figure 3. Considering that battery temperature T_{bat} and *SOC* can characterize the current state of the battery, they are selected as state variables with the following expressions:

$$ \dot{x} = \begin{bmatrix} \dot{SOC} \\ \dot{T}_{bat} \end{bmatrix} = \begin{bmatrix} \frac{I_{\mathrm{bat}}}{Q_{\mathrm{bat}} \cdot 3600} \\ \frac{{I_{\mathrm{bat}}}^2 \cdot R_{\mathrm{bat}} + P_{\mathrm{h}} \cdot \eta_{\mathrm{ptc}} - \mathrm{h} \cdot \mathrm{A} \cdot (T_{\mathrm{bat}} - \mathrm{T_{env}})}{c \cdot m} \end{bmatrix} \tag{5} $$

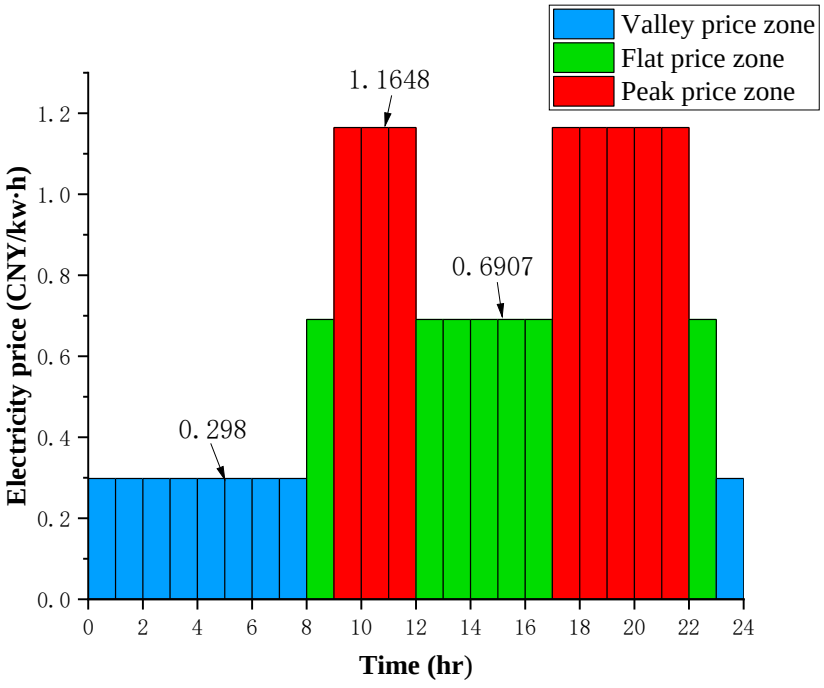

Figure 3. Time-of-use electricity prices in Hefei City.

The charging current I_{bat} and the electric power of the PTC heater P_{h} are selected as control variables, i.e., $u = [I_{\mathrm{bat}}; P_{\mathrm{h}}]^{\mathrm{T}}$.

For computer solving, dynamic programming requires discretization of the state system. Equations (3) and (4) provide the discrete expressions for battery *SOC* and temperature, respectively:

$$SOC(k+1) = SOC(k) + \frac{I_{\mathrm{bat}}(k)}{Q_{\mathrm{bat}} \cdot 3600} \cdot \Delta t \tag{6}$$

$$T_{bat}(k+1) = T_{bat}(k) + \frac{I_{\mathrm{bat}}(k)^2 \cdot R_{\mathrm{bat}}(x_k) + P_{\mathrm{h}}(k) \cdot \eta_{\mathrm{ptc}} - \mathrm{h} \cdot \mathrm{A} \cdot (T_{\mathrm{bat}}(k) - \mathrm{T_{env}})}{\mathrm{c} \cdot \mathrm{m}} \cdot \Delta t \tag{7}$$

Further, the state transfer equation of the system can be derived as follows:

$$x(k+1) = f(x(k), u(k)) \tag{8}$$

where $x(k)$ and $x(k+1)$ are the state variables at steps k and $(k+1)$ respectively, $u(k)$ is the control variable at step k, and $f(\cdot)$ is the system state transition equation function, which is expressed as follows:

$$f(x(k), u(k)) = x_k + \begin{bmatrix} \frac{I_{\mathrm{bat}}(k)}{Q_{\mathrm{bat}} \cdot 3600} \\ \frac{I_{\mathrm{bat}}(k)^2 \cdot R_{\mathrm{bat}}(x_k) + P_{\mathrm{h}}(k) \cdot \eta_{\mathrm{ptc}} - \mathrm{h} \cdot \mathrm{A} \cdot (T_{\mathrm{bat}}(k) - \mathrm{T_{env}})}{\mathrm{c} \cdot \mathrm{m}} \end{bmatrix} \cdot \Delta t \tag{9}$$

The control variables can be solved analytically based on the state transfer equation, which has the following expression:

$$\begin{bmatrix} I_{\mathrm{bat}}(k) \\ P_{\mathrm{h}}(k) \end{bmatrix} = \begin{bmatrix} \frac{SOC(k+1) - SOC(k)}{\Delta t} \cdot Q_{\mathrm{bat}} \cdot 3600 \\ \frac{(T_{\mathrm{bat}}(k+1) - T_{\mathrm{bat}}(k)) \cdot \mathrm{c} \cdot \mathrm{m} + \left(\mathrm{h} \cdot \mathrm{A} \cdot (T_{\mathrm{bat}}(k) - \mathrm{T_{env}}) - I_{\mathrm{bat}}(k)^2 \cdot R_{\mathrm{bat}}(x_k)\right) \cdot \Delta t}{\Delta t \cdot \eta_{\mathrm{ptc}}} \end{bmatrix} \tag{10}$$

Dynamic programming to solve the cost optimization problem under the time-of-use electricity price requires solving the optimal control sequence when the objective function is minimized, and the objective function expression is:

$$J = \sum_{k=1}^{N} L(x_k, u_k) \tag{11}$$

where $L(x_k, u_k)$ is the transient transfer cost of step k, and J is the total cost of the first N steps.

Considering mainly the electricity cost $L_{\mathrm{c}}(x_k, u_k)$ consumed by charging the battery and the electricity cost $L_{\mathrm{ph}}(x_k, u_k)$ consumed by the PTC heater to preheat the battery, the transient transfer cost expression for step k is as follows:

$$\begin{aligned} L(x_k, u_k) &= L_{\mathrm{c}}(x_k, u_k) + L_{\mathrm{ph}}(x_k, u_k) \\ &= c_{ele}(k) \cdot (I_{\mathrm{bat}}(k) \cdot (U_{\mathrm{ocv}}(x_k) + I_{\mathrm{bat}}(k) \cdot R_{\mathrm{bat}}(x_k)) + P_{\mathrm{h}}(k)) \cdot \frac{\Delta t}{3.6 \cdot 10^6} \end{aligned} \tag{12}$$

where $c_{ele}(k)$ is the electricity price at step k.

Considering the thermal safety during the battery charging–preheating process and the power limitations of the PTC heater, the following constraints are imposed mainly on the battery *SOC*, the battery temperature T_{bat}, the AC charging current I_{bat}, and the power of the PTC heater P_{h}:

$$\begin{cases} \mathrm{SOC_{init}} \le SOC \le 95\% \\ \mathrm{T_{env}} \le T_{\mathrm{bat}} \le 35\ ^{\circ}\mathrm{C} \\ 0\ \mathrm{A} \le I_{\mathrm{bat}} \le 30\ \mathrm{A} \\ 0\ \mathrm{W} \le P_{\mathrm{h}} \le 7000\ \mathrm{W} \end{cases} \tag{13}$$

where $\mathrm{SOC_{init}}$ is the initial *SOC* of the battery.

The initial temperature of the battery pack is the ambient temperature, and the user can set the target temperature and *SOC* under the reserved departure time. Considering the suitable working temperature range of Li-ion batteries is 15~35 °C [28,29], the target temperature is set to 25 °C, and the target *SOC* is set to 95%. The AC charging current and power of the PTC heater are adjusted according to the user's target departure time and time-of-use electricity price, which not only meets the user's charging–preheating demand but also reduces the user's cost.

$$\begin{cases} SOC(1) = \mathrm{SOC_{init}} \\ T_{\mathrm{bat}}(1) = \mathrm{T_{env}} \\ SOC(N) = \mathrm{SOC_{bat,tar}} \\ T_{\mathrm{bat}}(N) = \mathrm{T_{bat,tar}} \end{cases} \tag{14}$$

where $\mathrm{SOC_{bat,tar}}$ is the target *SOC* of the battery, and $\mathrm{T_{bat,tar}}$ is the target temperature of the battery.

3.2. Dynamic Programming Solution

Dynamic programming algorithms are widely used in hybrid vehicle energy management systems to obtain global optimal control strategies for given driving cycles [30,31]. The algorithm can convert a multi-stage decision-making problem into a series of single-stage decision-making problems, which are gradually solved inversely from back to front according to the state transfer equation. As shown in Figure 4, the battery's initial and termination states are fixed, and the user's target departure time is set to t_{desire}. The state variables and time domain are discretized, and the discrete state mesh shown in Figure 4 can be obtained. Among them, the simulation step Δt is set to 600 s, and the number of discrete grids in the time domain is $\frac{t_{\mathrm{desire}}}{\Delta t} + 1$. The number of discrete grids for battery temperature and *SOC* is 201, and the discretization accuracies of the battery temperature and *SOC* are 0.2736 °C and 0.0037, respectively. The specific solution process of dynamic programming is shown in Figure 5, in which some variables are defined as follows: ${x_m}^{i,j}$ represents the state at the position in the grid (i, j) at the $k = m$ step, ${u_m}^{q}$ represents the q-th control variable of ${x_m}^{i,j}$ at the $k = m$ step, $L\left({x_m}^{i,j}, {u_m}^{q}\right)$ is the instantaneous transfer cost of state ${x_m}^{i,j}$ with input control variable ${u_m}^{q}$, $J\left({x_m}^{i,j}, {u_m}^{q}\right)$ is the remaining cost of state ${x_m}^{i,j}$ to terminate state with input control variable ${u_m}^{q}$ at the $k = m$ step, $J^*(x_m)$ is the minimum remaining cost of state x_m at the $k = m$ step, and $u^*(x_m)$ is the optimal control sequence of state x_m at the $k = m$ step.

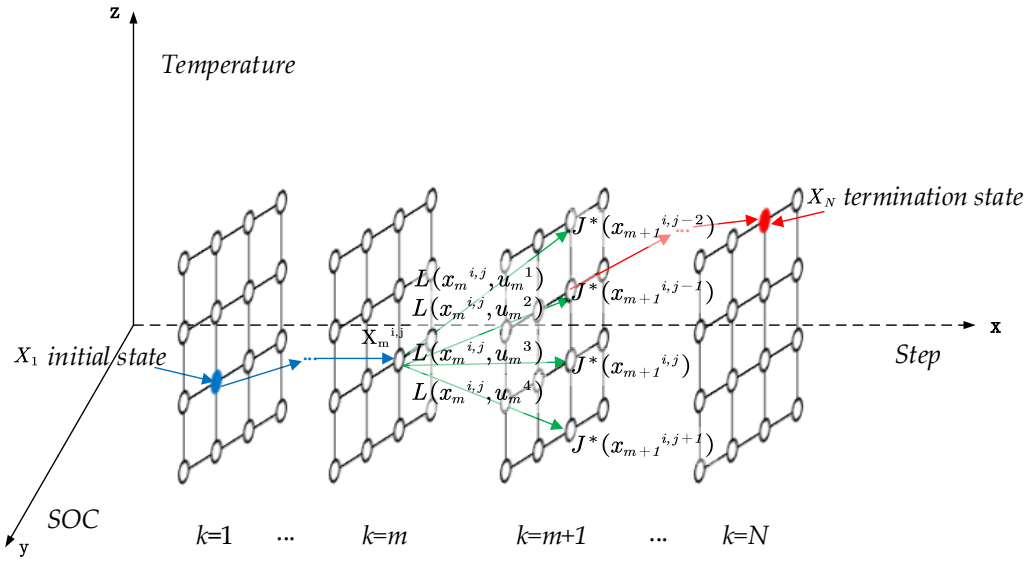

Figure 4. Principle diagram of the dynamic programming algorithm.

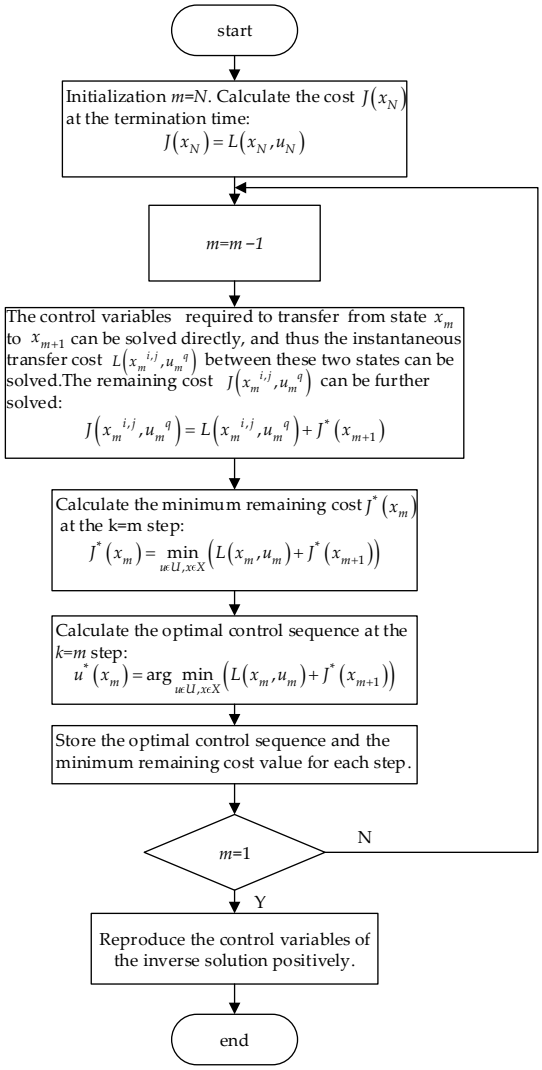

Figure 5. Flow chart of the dynamic programming solution.

4. Results and Discussion

4.1. Conventional Preheating Strategy

As shown in Figure 6, most electric vehicle owners choose to charge at night. The battery is left in the environment for a long time after charging, and the battery temperature becomes the same as the ambient temperature. Before traveling, the high-power PTC heater is turned on to heat the battery to the target temperature. The conventional preheating strategy does not utilize the time-of-use electricity price or charging waste heat. In addition, the grid cost consumed by the PTC heater is closely related to the user's travel time. For example, when the user travels in the peak price zone, the grid cost consumed by the PTC heater is much higher than that in the valley price zone.

When the battery remains in the environment after charging for a long time, the heat produced by the charging internal resistance in the conventional preheating strategy is negligible (assuming I_{bat} is set to 0), and the temperature rise function of the battery is derived from Equation (3):

$$T_{\mathrm{bat}}=\frac{P_{\mathrm{h}}\cdot\eta_{\mathrm{ptc}}\cdot\left(1-e^{-\frac{\mathrm{A}\cdot\mathrm{h}\cdot t}{\mathrm{c}\cdot\mathrm{m}}}\right)+\mathrm{h}\cdot\mathrm{A}\cdot\mathrm{T}_{\mathrm{env}}}{\mathrm{h}\cdot\mathrm{A}} \tag{15}$$

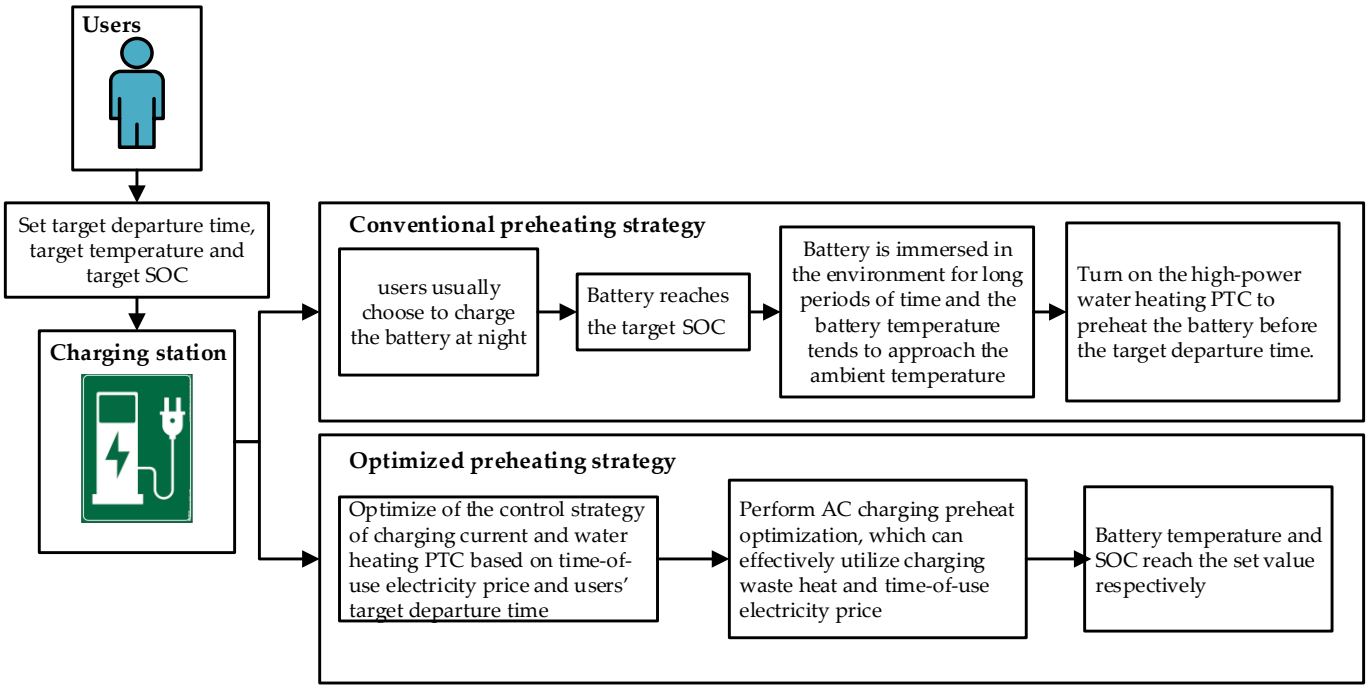

Figure 6. Flowchart of the conventional preheating strategy and optimized preheating strategy.

The battery preheating target temperature is set to 25 °C. The maximum power of the PTC heater is 7000 W. Further, according to the above equation, the preheating time and energy consumption required for the conventional preheating strategy at different ambient temperatures can be found. The results are shown in Table 4.

Table 4. Preheating time and energy consumption under different ambient temperatures.

Ambient Temperature/°C	Preheating Time/s	Energy Consumption/(kw·h)
−20	2008.4	3.91
−15	1779.7	3.46
−10	1552.5	3.02
−5	1326.6	2.58
0	1102.1	2.14

The cost of the conventional preheating strategy is solved by integrating the grid energy consumed to heat the battery during the preheating time and the time-of-use electricity price for that period:

$$c_{\text{heat,now}} = \int_{t_{\text{desire}}-t_{\text{heat,now}}}^{t_{\text{desire}}} c_{\text{ele}}(t) \cdot P_{\text{h,max}} \mathrm{d}t \tag{16}$$

where $c_{\text{heat,now}}$ is the cost of the conventional preheating strategy, t_{desire} is the user's target departure time, $t_{\text{heat,now}}$ is the preheating time for the conventional preheating strategy, $c_{\text{ele}}(\cdot)$ is the time-of-use electricity price function, and $P_{\text{h,max}}$ is the maximum power of the PTC heater.

The cost-saving rate can be calculated based on the cost of the optimized strategy and the cost of the conventional preheating strategy with the following expression:

$$c_{\text{rate}} = \frac{c_{\text{heat,now}} - J^*(x_1)}{c_{\text{heat,now}}} \times 100\% \tag{17}$$

where c_{rate} is the cost-saving rate, and $J^*(x_1)$ is the cost of the optimized preheating strategy.

4.2. Comparison and Analysis of Simulation Results

This study used the MATLAB (R2022b) simulation platform to complete the modeling of the thermal management system and the realization of optimal control, and then draws the following conclusions. The optimized total cost increases as the ambient temperature decreases and the user's target departure time increases, as shown in Figure 7. This is because colder temperatures require more electrical energy to heat the battery to the target temperature. If the target departure time is delayed, the heat generated by preheating the battery during the valley price period will gradually dissipate. For the battery to reach the set temperature value, it needs to increase the turn-on time of the PTC heater in the flat and peak zones, so the total cost consumption is higher.

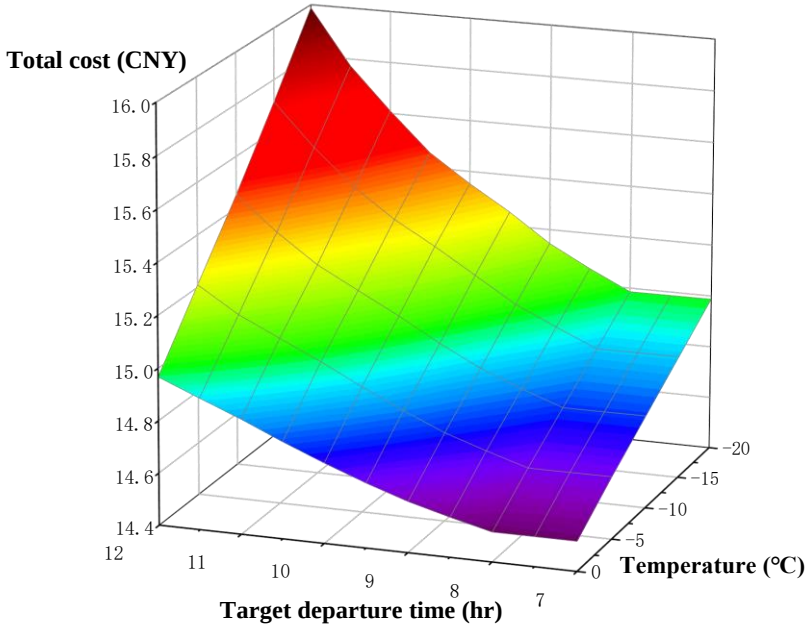

Figure 7. Total cost of the optimized preheating strategy.

The result of the optimized control strategy, when the ambient temperature is −20 °C and the user's target departure time is 11:30, is shown in Figure 8. During the AC charging process, the battery pack reaches the set target *SOC* at 8:00, and the charging current is 0 after 8:00. This is because charging with a large capacity of Li-ion batteries consumes high electrical energy, and charging in the valley price zone is more economical. From the curve of the battery temperature, it can be seen that the rise in the battery temperature before 8:00 is mainly due to the heat generated by the internal resistance of the battery during the charging process and the heat production of the PTC heater in the valley price zone. To ensure that the battery temperature reaches 25 °C at 11:30 with the lowest cost, the optimized control strategy turns on the high-power PTC heater in the valley price zone to heat the battery to the set upper-temperature threshold, Tbat_max; it then cools it down in the ambient temperature, and continues to turn on the PTC heater in the flat price zone to heat the battery to Tbat_max, and repeats the cooling-down process afterward. Finally, turning on the PTC heater with a small amount of power in the peak price zone makes the battery reach 25 °C under the combined effect of the ambient temperature and the PTC heater. At this time, the power consumed by preheating the battery is mainly concentrated in the valley and flat price zones. In contrast, the conventional preheating strategy uses the PTC heater with a large amount of power to heat the battery before 11:30, concentrating all the power consumption in the peak price area.

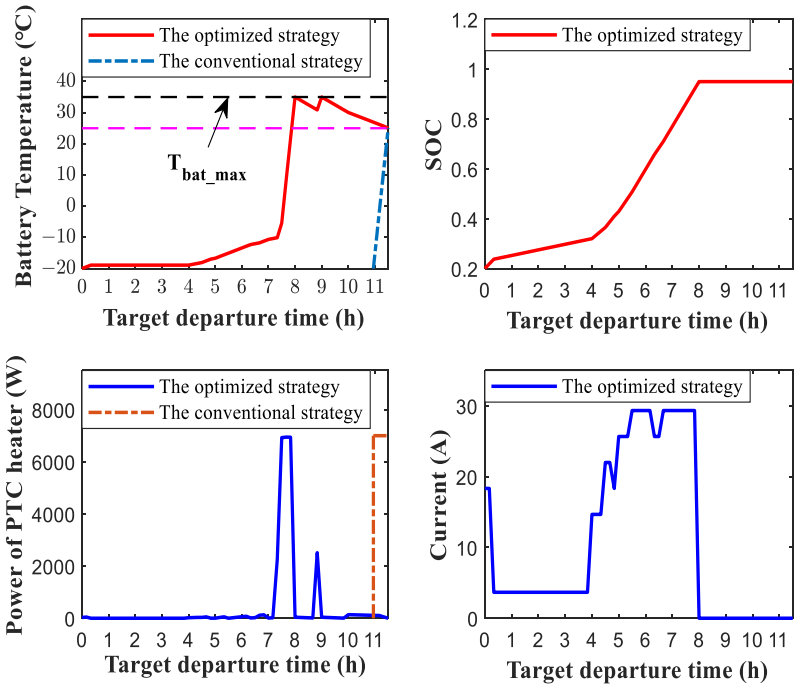

Figure 8. Simulation results for −20 °C temperature and 11:30 target departure time.

The comparison of the grid cost consumed by the conventional preheating strategy and the optimized strategy is shown in Figure 9. From Equation (16), the cost of the conventional preheating strategy is mainly affected by the electricity price under the user's target traveling time and the energy consumption of the battery preheating. Under the same ambient temperature, the trend of the cost of the conventional preheating strategy over time is consistent with the trend of the time-of-use electricity price over time. That is, the cost of the conventional preheating strategy remains constant in each region of the valley price zone (0:00 to 8:00), the flat price zone (8:00 to 9:00), and the peak price zone (9:00 to 12:00), but the cost of preheating decreases sequentially between different regions of the time-of-use electricity price. The preheating cost of the optimized strategy follows the same trend as the optimized strategy's total cost, increasing with decreasing ambient temperature and increasing target departure times.

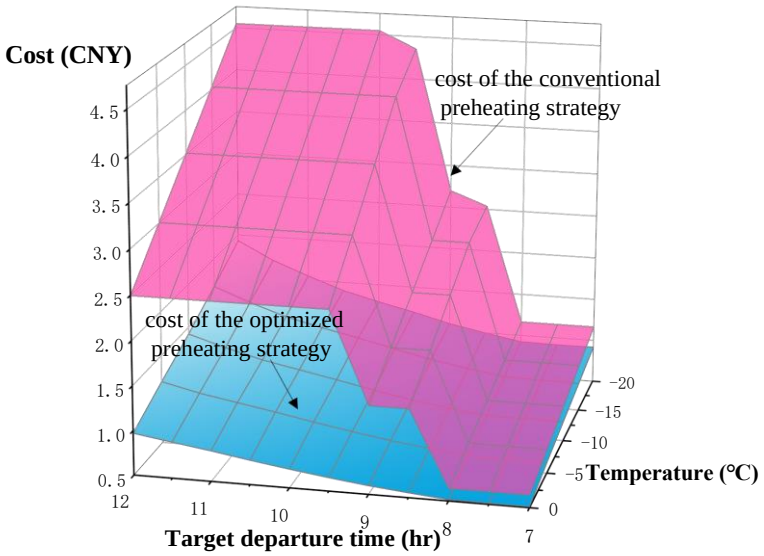

Figure 9. Cost comparison between the optimized and conventional preheating strategy.

The grid cost savings of the optimized strategy compared to the conventional preheating strategy are shown in Table 5. Under the ambient temperature of −15 °C to 0 °C, the optimized strategy generally saves the highest cost when the user's target travel time is 9:30. The highest cost saving is CNY 3.26 at −20 °C. Under the ambient temperature of −20 °C to 0 °C, the cost savings are generally lowest when the user's target departure time is set to 8:00, and there is little difference in the cost savings before 8:00. This is because the valley price zones are all before 8:00, and the differences in charging strategies between different target departure times lead to small changes in the turn-on time of the PTC heater.

Table 5. Cost savings of the optimized control strategy.

Target Departure Time/h	Ambient Temperature/°C				
	−20	−15	−10	−5	0
7:00	0.25	0.21	0.18	0.15	0.13
7:30	0.25	0.21	0.18	0.14	0.13
8:00	0.24	0.20	0.18	0.14	0.12
8:30	1.54	1.49	1.31	1.11	0.93
9:00	1.61	1.42	1.25	1.05	0.88
9:30	3.16	2.96	2.60	2.21	1.85
10:00	3.26	2.86	2.50	2.13	1.79
10:30	3.15	2.77	2.42	2.05	1.72
11:00	3.00	2.67	2.34	1.98	1.65
11:30	2.84	2.52	2.22	1.90	1.59
12:00	2.62	2.36	2.09	1.80	1.53

The results of the optimized control strategy are shown in Figure 10 when the ambient temperature is −15 °C and the user's target departure time is 9:30. At this time, the energy consumption of the PTC heater is mainly concentrated in the valley price zone. After the battery temperature increases to 29.5 °C, the ambient heat dissipation begins and the battery temperature eventually decreases to 25 °C. The heating moment interval of the conventional preheating strategy is all in the flat price zone. Thus, the cost savings are generally higher when the target departure time is 9:30.

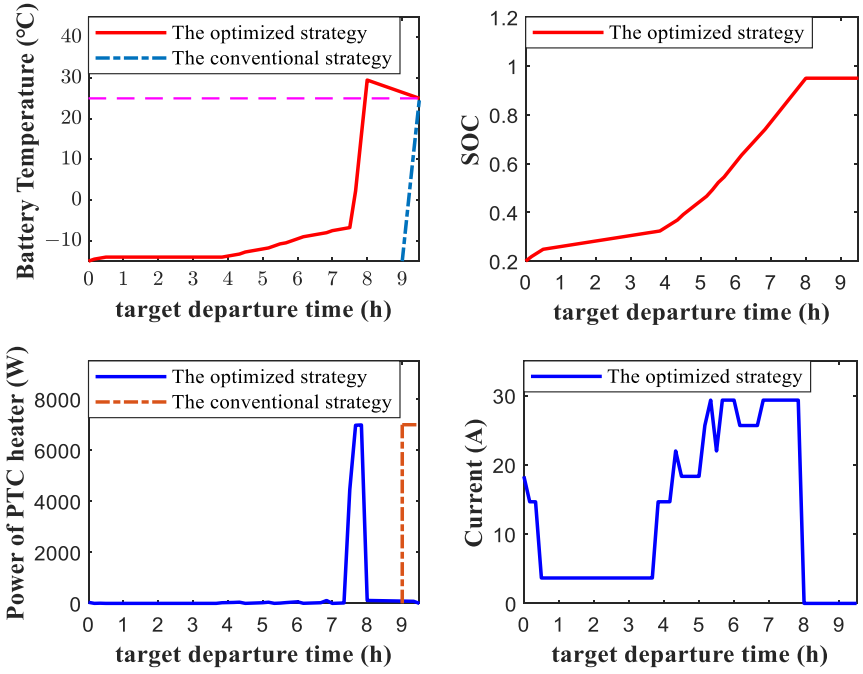

Figure 10. Simulation results for −15 °C temperature and 9:30 target departure time.

The optimized cost-saving rate at different ambient temperatures is shown in Figure 11. The cost-saving rate ranges from 18.41% to 73.96%. Under the ambient temperature of −20 °C to 0 °C, the cost-saving rate before 8:00 is about 20%. This is because the conventional preheating strategy relies solely on the PTC heater to preheat the battery to the target temperature. In contrast, the appointment charging and battery preheating are performed simultaneously, as proposed in this paper. The internal resistance heat production of the battery during the charging process reduces the turn-on time of the PTC heater, resulting in a higher cost utilization of the optimized strategy than the conventional preheating strategy.

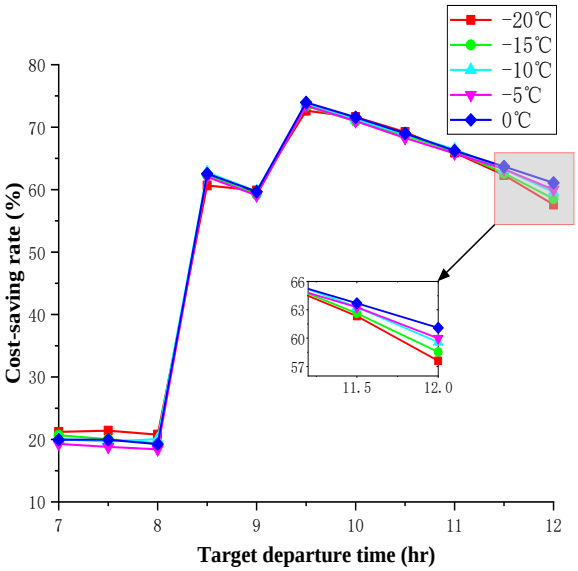

Figure 11. Cost-saving rate of the optimized preheating strategy.

Under the ambient temperature of −20 °C to 0 °C, the cost savings after 8:00 are more significant than those before 8:00. This is because the optimized control strategy makes full use of the valley price zone of the time-of-use electricity price. In contrast, most of the turn-on periods of the PTC heater in the conventional preheating strategy are concentrated in the flat or peak price zones.

5. Conclusions

Reasonable use of the TOU price can effectively save the cost of the user's power network. At present, most studies focus on the effect of the TOU on charging, but the novelty of this paper is to study the effect of the TOU on the preheating strategy of the battery, while considering the waste heat generated by the slow charging current under the TOU. In this paper, battery thermodynamic and *SOC* models are built based on the integrated thermal management system scheme. Aiming at the scenario of pure electric vehicles using charging piles for AC charging and battery preheating, a method based on the time-of-use electricity price for optimizing AC charging current and the control strategy of the PTC heater is proposed. The effectiveness of the method in terms of cost saving is also analyzed under different ambient temperatures and the user's target departure times.

The simulation results show that the optimized control strategy can make the battery reach the desired *SOC* and temperature at the target departure time with the lowest total cost. In addition, the optimized AC charging–preheating total cost increases with decreasing ambient temperature and increasing target travel moment. Compared with the conventional preheating strategy, the optimized battery preheating strategy can save up to CNY 3.26 at different ambient temperatures and users' target departure times, and the cost-saving rate can reach from 18.41% to 73.96%. Under −15~0 °C, the cost utilization rate reaches the maximum value at 9:30, which can effectively utilize the grid energy in the

valley price zone and reduce the effective turn-on time of the PTC heater in the flat price zone.

The main limit of this article is that the impact of parking fees and declining battery life on users' cost is not considered. Our further work will focus more on the comprehensive cost optimization caused by user travel patterns and battery life aging during the charging process.

Author Contributions: Conceptualization, B.Z.; methodology, M.Y.; software, Z.Q.; validation, M.Y.; formal analysis, C.B.; investigation, B.Z.; resources, C.B.; data curation, M.Y.; writing—original draft preparation, C.B.; writing—review and editing, C.B.; visualization, Z.Q.; supervision, M.Y.; project administration, B.Z.; funding acquisition, B.Z. All authors have read and agreed to the published version of the manuscript.

Funding: This research was funded by [Anhui Provincial Natural Science Foundation Project] grant number [2308085ME159].

Data Availability Statement: No new data were created or analyzed in this study. Data sharing is not applicable to this article.

Conflicts of Interest: The authors declare no conflict of interest.

References

1. Lei, S.; Xin, S.; Liu, S. Separate and integrated thermal management solutions for electric vehicles: A review. *J. Power Sources* **2022**, *550*, 232133. [CrossRef]
2. Wang, J.; Ruan, L. Performance investigation of integrated thermal management system based on a pumped two-phase cooling system for electric vehicles. *J. Energy Storage* **2023**, *72*, 107922. [CrossRef]
3. Ye, J.; Aldaher, A.Y.M.; Tan, G. Thermal performance analysis of 18,650 battery thermal management system integrated with liquid-cooling and air-cooling. *J. Energy Storage* **2023**, *72*, 108766. [CrossRef]
4. Dai, X.; Ping, P.; Kong, D.; Gao, X.; Zhang, Y.; Wang, G.; Peng, R. Heat transfer enhanced inorganic phase change material compositing carbon nanotubes for battery thermal management and thermal runaway propagation mitigation. *J. Energy Chem.* **2023**, *89*, 226–238. [CrossRef]
5. Huang, Z.; Gao, Z.; Liu, Y.; Guan, K.; Lu, Y.; Zhou, F.; Jiang, F.; Peng, J. A low temperature preheating strategy with optimized fuzzy controller for lithium-ion batteries. *J. Energy Storage* **2022**, *52*, 104709. [CrossRef]
6. Zhang, C.; Huang, J.; Sun, W.; Xu, X.; Li, C.; Li, Y. Research on liquid preheating performance for battery thermal management of electric vehicles at low temperature. *J. Energy Storage* **2022**, *55*, 105497. [CrossRef]
7. Wang, Y.; Zhang, X.; Chen, Z. Low temperature preheating techniques for Lithium-ion batteries: Recent advances and future challenges. *Appl. Energy* **2022**, *313*, 118832. [CrossRef]
8. Ruan, H.; Jiang, J.; Sun, B.; Su, X.; He, X.; Zhao, K. An optimal internal-heating strategy for lithium-ion batteries at low temperature considering both heating time and lifetime reduction. *Appl. Energy* **2019**, *256*, 113797. [CrossRef]
9. Zhu, J.; Sun, Z.; Wei, X.; Dai, H.; Gu, W. Experimental investigations of an AC pulse heating method for vehicular high power lithium-ion batteries at subzero temperatures. *J. Power Sources* **2017**, *367*, 145–157. [CrossRef]
10. Wu, X.; Cui, Z.; Chen, E.; Du, J. Capacity degradation minimization oriented optimization for the pulse preheating of lithium-ion batteries under low temperature. *J. Energy Storage* **2020**, *31*, 101746. [CrossRef]
11. Chen, S.; Zhang, G.; Wu, C.; Huang, W.; Xu, C.; Jin, C.; Wu, Y.; Jiang, Z.; Dai, H.; Feng, X.; et al. Multi-objective optimization design for a double-direction liquid heating system-based Cell-to-Chassis battery module. *Int. J. Heat Mass Transf.* **2022**, *183*, 122184. [CrossRef]
12. Qin, P.; Sun, J.; Yang, X.; Wang, Q. Battery thermal management system based on the forced-air convection: A review. *eTransportation* **2021**, *7*, 100097. [CrossRef]
13. Qin, P.; Liao, M.; Mei, W.; Sun, J.; Wang, Q. The experimental and numerical investigation on a hybrid battery thermal management system based on forced-air convection and internal finned structure. *Appl. Therm. Eng.* **2021**, *195*, 117212. [CrossRef]
14. Wang, Y.; Rao, Z.; Liu, S.; Li, X.; Li, H.; Xiong, R. Evaluating the performance of liquid immersing preheating system for Lithium-ion battery pack. *Appl. Therm. Eng.* **2021**, *190*, 116811. [CrossRef]
15. Huang, Y.-H.; Cheng, W.-L.; Zhao, R. Thermal management of Li-ion battery pack with the application of flexible form-stable composite phase change materials. *Energy Conv. Manag.* **2019**, *182*, 9–20. [CrossRef]
16. Li, X.; Deng, J.; Huang, Q.; Zhang, G.; Chen, K.; Wang, Y. Experimental investigation on immersion liquid cooled battery thermal management system with phase change epoxy sealant. *Chem. Eng. Sci.* **2022**, *264*, 118089. [CrossRef]
17. Luo, M.; Ling, Z.; Zhang, Z.; Fang, X. A fast-response preheating system coupled with supercapacitor and electric conductive phase change materials for lithium-ion battery energy storage system at low temperatures. *J. Energy Storage* **2023**, *73*, 109255. [CrossRef]

18. Liu, X.; Hong, X.; Jiang, X.; Li, Y.; Xu, K. Novel approach for liquid-heating lithium-ion battery pack to shorten low temperature charge time. *J. Energy Storage* **2023**, *68*, 107507. [CrossRef]
19. Antoun, J.; Kabir, M.E.; Atallah, R.; Moussa, B.; Ghafouri, M.; Assi, C. Assisting Residential Distribution Grids in Overcoming Large-Scale EV Preconditioning Load. *IEEE Syst. J.* **2022**, *16*, 4345–4355. [CrossRef]
20. Sørensen, Å.L.; Ludvigsen, B.; Andresen, I. Grid-connected cabin preheating of Electric Vehicles in cold climates–A non-flexible share of the EV energy use. *Appl. Energy* **2023**, *341*, 121054. [CrossRef]
21. Liang, S.; Zhu, B.; He, J.; He, S.; Ma, M. A pricing strategy for electric vehicle charging in residential areas considering the uncertainty of charging time and demand. *Comput. Commun.* **2023**, *199*, 153–167. [CrossRef]
22. Tian, X.; Cheng, B.; Liu, H. V2G optimized power control strategy based on time-of-use electricity price and comprehensive load cost. *Energy Rep.* **2023**, *10*, 1467–1473. [CrossRef]
23. Yin, W.; Wen, T.; Zhang, C. Cooperative optimal scheduling strategy of electric vehicles based on dynamic electricity price mechanism. *Energy* **2023**, *263*, 125627. [CrossRef]
24. Ouyang, Q.; Fang, R.; Xu, G.; Liu, Y. User-involved charging control for lithium-ion batteries with economic cost optimization. *Appl. Energy* **2022**, *314*, 118878. [CrossRef]
25. Guo, R.; Li, L.; Sun, Z.; Xue, X. An integrated thermal management strategy for cabin and battery heating in range-extended electric vehicles under low-temperature conditions. *Appl. Therm. Eng.* **2023**, *228*, 120502. [CrossRef]
26. Hou, J.; Xu, J.; Lin, C.; Jiang, D.; Mei, X. State of charge estimation for lithium-ion batteries based on battery model and data-driven fusion method. *Energy* **2024**, *290*, 130056. [CrossRef]
27. Wu, M.; Qin, L.; Wu, G. State of power estimation of power lithium-ion battery based on an equivalent circuit model. *J. Energy Storage* **2022**, *51*, 104538. [CrossRef]
28. Shahjalal, M.; Shams, T.; Islam, M.E.; Alam, W.; Modak, M.; Hossain, S.B.; Ramadesigan, V.; Ahmed, M.R.; Ahmed, H.; Iqbal, A. A review of thermal management for Li-ion batteries: Prospects, challenges, and issues. *J. Energy Storage* **2021**, *39*, 102518. [CrossRef]
29. Liu, J.; Yadav, S.; Salman, M.; Chavan, S.; Kim, S.C. Review of thermal coupled battery models and parameter identification for lithium-ion battery heat generation in EV battery thermal management system. *Int. J. Heat Mass Transf.* **2024**, *218*, 124748. [CrossRef]
30. Wang, C.; Liu, F.; Tang, A.; Liu, R. A dynamic programming-optimized two-layer adaptive energy management strategy for electric vehicles considering driving pattern recognition. *J. Energy Storage* **2023**, *70*, 107924. [CrossRef]
31. Li, F.; Gao, L.; Zhang, Y.; Liu, Y. Hierarchical operation switch schedule algorithm for energy management strategy of hybrid electric vehicle using adaptive dynamic programming. *Sustain. Energy Grids Netw.* **2023**, *35*, 101107. [CrossRef]